THE JOURNAL OF PHYSICAL CHEMISTRY B

Article

pubs.acs.org/JPCB

Rigid Body Brownian Dynamics as a Tool for Studying Ion Channel Blockers

Dan Gordon,*[,†] Rong Chen,[†] Junming Ho,[‡] Michelle L. Coote,[‡] and Shin-Ho Chung[†]

[†]Research School of Biology, Australian National University, Canberra, Australia

[‡]Research School of Chemistry, Australian National University, Canberra, Australia

Supporting Information

ABSTRACT: Using a novel rigid body Brownian dynamics algorithm, we investigate how a spherically asymmetrical polyamine molecule, a branched analogue of spermine, interacts with the external vestibule of the voltage-gated potassium channel, Kv1.2. Simulations reveal that the blocker, with a charge of +4*e*, inserts one of its charged amine groups into the selectivity filter, while another forms a salt bridge with an aspartate residue located just outside the entrance of the pore. This binding mode mimics features of the binding of polypeptides such as the scorpion venom charybdotoxin to the channel. The potential of mean force constructed with Brownian dynamics is a reasonable match to that obtained from molecular dynamics simulations, with dissociation constants of 4.7 and 22 μM, respectively. The current−voltage relationships obtained with and without a blocker in the external reservoir show that the inward current is severely attenuated by the presence of the blocker, whereas the outward current is only moderately reduced. The computational molecular modeling technique we introduce here can provide detailed insights into ligand−channel interactions and can be used for rapidly screening potential blocker molecules.

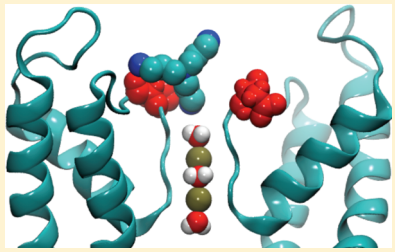

INTRODUCTION

The conduction of ions across voltage-gated potassium channels may be attenuated by the presence of blocker molecules, which intermittently bind to the channel and physically occlude the pore. These blocker molecules can range in size from small, compact charged molecules such as 4-aminopyridine or tetraethylammonium to the large polypeptides commonly found in various kinds of toxins that are produced, for example, by spiders, snakes, scorpions, cone shells, and sea anemones. Studying how these compounds bind to and block ion channels has provided many useful insights about the mechanisms of ion conduction, the structure of external vestibules, and the mechanistic basis for phenotypic differences among channels.

There also exists the potential for channel blockers to treat disease, in cases where the pathology results from an elevated conduction through a particular channel.[1] For example, an overexpression of the Kv1.3 channel in T-cells is implicated in a variety of autoimmune diseases including multiple sclerosis, type 1 diabetes, and rheumatoid arthritis. The ability to selectively block this channel may therefore lead to new treatments for these conditions; various selective small molecule (e.g., clofazimine[2]) and polypeptide toxin (e.g., ShK and its derivatives[3−6]) Kv1.3 blockers are currently known.

The potential for channel blockers to treat disease renders them an important target for computational modeling. However, the problem is particularly challenging, as we would like to be able to rapidly screen candidate blocker compounds, to be able to assess blocking effectiveness, and to take into account the particular electrostatics found in ion channels, dependent as they are on long time scale movements of a small number of key ions that dwell within the channel. Currently, docking and molecular dynamics are often used to study the interactions between blockers and channels, often in conjunction with each other. Docking fulfills the requirement for rapid screening of compounds and may provide an important tool for initial testing.[7,8] Many of the docking systems, however, are more suitable for studying the binding of small ligands to a substrate and in an ion channel environment may neglect important details about the electrostatics and particularly the ions that dwell inside the pore. Furthermore, the results do not necessarily give an accurate indication of actual blocking effectiveness or of the kinetics of blocking and unblocking. Molecular dynamics is often used to refine and test a candidate docked configuration produced by a docking program. While we can hope for an accurate representation of the binding free energy and dynamics of the blocker, the computational resources needed can provide a bottleneck, and currently it is very difficult to produce trajectories at the time scales on which ionic conduction occurs.

In this paper, we investigate the use of Brownian dynamics as a computational tool for studying the interaction between ion channels and channel blockers. We see Brownian dynamics as combining desirable features of docking and molecular dynamics that may be able to provide relatively rapid screening of compounds while also elucidating the mechanisms and

Received: October 21, 2011
Revised: December 13, 2011
Published: January 18, 2012

dynamics of block and unblock. We have devised a rigid body Brownian dynamics algorithm that can simulate the tumbling motion of blocker molecules and have incorporated this algorithm and other changes into our Brownian dynamics code. We employ the Kv1.2 channel, for which a crystal structure exists,[9] and use as a test blocker a branched analogue of spermine, a polyamine molecule with a charge of +4*e* at neutral pH. We have chosen to study this particular model because it is a small, relatively rigid molecule that appears to bind to the external vestibule of the channel in a way that mimics some of the features of the larger polypeptide binding modes:[10−17] there is an overall electrostatic attraction to the negatively charged outer vestibule due to the charge of +4*e* combined with the insertion of one charged amine group into the mouth of the channel and the interaction and formation salt bridges with another with a negatively charged aspartate residue just outside the entrance to the pore. Once the methodology proves feasible, it should be possible to develop new blockers either from the ground up, by selectively adding new groups to small molecules and rapidly testing the new molecules, or from top down, by selectively pruning groups from large molecules and similarly testing the effect of the changes.

Here, we present initial results of our Brownian dynamics system. We find using molecular dynamics simulations that this molecule does indeed appear to bind to the pore in this manner. We then carry out Brownian dynamics simulations to model the process of block. Comparing potentials of mean force (PMFs) between Brownian and molecular dynamics, we find that the depth of the binding well as well as the shape of the unbound section of the PMFs match remarkably well, but that there is some discrepancy in the details of the interaction as the blocker approaches the channel. We go on to examine the actual blocking effectiveness of the molecule. The compound does indeed block the current in the physiological range, with both the magnitude of the current and the shape of the *I*−*V* curve being affected by its presence. Relative to the control curve, the blocker causes the channel to become outward rectifying. At 320 mM KCl concentration and ∼20 mM blocker concentration in the external reservoir, the blocking effectiveness is 74% at −100 mV and 33% at +100 mV.

THEORY AND METHODS

Modeling and Equilibration of the Channel. We build an initial channel model which is used as a starting point for both Brownian and molecular dynamics simulations. We model the Kv1.2 channel based on the protein data bank crystal structure 2A79 obtained by Long et al.[9] The VMD molecular viewing and modeling program[18] and the NAMD molecular dynamics program[19] are used to build the model systems. To optimize computational resources, we use a neutral segment of the protein that surrounds the pore and includes residues 288−420. We construct a tetramer based on crystallographic symmetry operations and add potassium ions and water in the selectivity filter, with the ions lying in binding sites S0 (just above Tyr377), S2 (between Val375 and Gly376), and S4 (between Thr374 and Thr373).[20]

For use in molecular dynamics simulations, we surround the tetramer by a lipid bilayer containing 109 1-palmitoyl-2-oleoyl-*sn*-glycero-3-phosphocholine (POPC) molecules and hydrate with a 250 mM KCl solution containing 13 629 water molecules and 67 each of K^+ and Cl^- ions. After equilibration, the unit cell has dimensions 76 Å × 76 Å × 106 Å, with the *z*-axis being parallel to the pore axis. The system is equilibrated using NAMD with the CHARMM22/27/CMAP force field.[21,22] A Langevin thermostat is used to control the temperature, with a damping constant of 1 ps^{-1} and a temperature of 310 K. We employ constant pressure dynamics at 1 atm using a Nosé-Hoover Langevin piston, with the cell shape fixed to a square in the *x*−*y* plane. Periodic boundary conditions are incorporated using particle mesh Ewald electrostatics. In order to confine the lipid bilayer to the center of the simulation cell, we constrain its center of mass in the *z*-direction, using a harmonic force with a spring constant 0.2 kcal/mol $Å^2$. The *x*−*y* motion of the protein center of mass is likewise constrained, using the same spring constant. Initially, the protein is fixed and the lipids, water, and ions are allowed to equilibrate around the fixed protein. Following this, some 10 ns of molecular dynamics are performed using only the constraints described above, with the first 5 ns being considered equilibration and the second 5 ns being considered a production run to be used for the analysis of rmsd etc. as discussed in the Results section.

For the construction of a channel model for use in Brownian dynamics, we derive a time-averaged symmetrized structure based on the molecular dynamics equilibration. The equilibration frames are first translated and rotated in order to best align them to the initial structure. The monomers are each rotated by a multiple of 90° so that they are all in alignment, and an average structure is calculated over all equilibration frames. The symmetrized tetramer is then reconstructed by rerotating back to the original orientations of the monomers. This structure is used to provide constraints for constrained minimization/refinement of the tetramer in order to derive a single physically reasonable structure that in some way represents the mean structure.

Blocker Model. On the basis of the binding mechanism of charybdotoxin and other peptide toxins, we surmise that partially effective attenuation of inward and outward currents of several Kv channels can be achieved by blockers that insert one amine group (like lysine) into the entrance to the pore while binding with another group or groups to the negatively charged aspartate residues that surround the pore. We therefore investigate a branched analogue of the spermine molecule, tris(3-aminopropyl)amine, which has a charge of +4 *e* at neutral pH and chemical formula, $C_{12}H_{28}N_4$, shown in Figure 1. The putative binding mode has one lysine like branch inserting in the pore while another interacts with one of the aspartate residues that surround the pore.

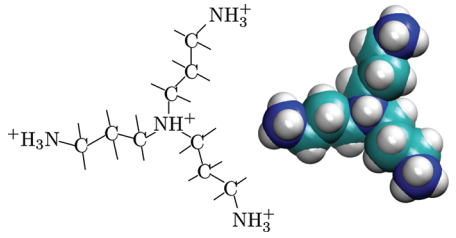

Figure 1. The blocker molecule, tris(3-aminopropyl)amine (in protonated state), $C_{12}H_{28}N_4$, a branched analogue of spermine and also having a charge of +4*e*.

The blocker geometry is optimized using Gaussian03[23] at the B3LYP/6-31+G(d) level of theory. The associated atomic charges are generated using the NBO scheme[24−26] at the

B3LYP/6-311+G(d,p) level in the presence of a solvent field, where the CPCM-UAKS[27,28] continuum solvent model was employed. In order to maintain maximum compatibility with the CHARMM27 force field and because the three legs of the blocker resemble lysine, the charges on the legs are then modified to match those of lysine while maintaining the calculated charges for the central group. Although the pK_as of this compound appear not to be known, we assume based on those of spermine (which has an average charge of 3.8 at pH = 7) that it should be nearly full protonated at neutral pH, with an average charge somewhere between +3e and +4e. Thus, we use the +4 protonation state in our simulations.

Details of the Brownian Dynamics Simulation. In our Brownian dynamics code, only the ions and rigid blocker molecules are explicitly simulated. The movable bodies are confined within a cylindrical simulation cell. The channel and lipid bilayer are treated as a fixed, rigid entity which runs across the center of the simulation cell, dividing it into reservoir regions connected by the channel itself. The simulation cell is shown in Figure 2. A boundary is defined between the interior of the protein and the aqueous region, which acts both as a dielectric boundary for the purpose of solving Poisson's equation as well as a physical boundary that confines the simulation bodies to the aqueous region. Note that we employ Poisson's equation, rather than the Poisson–Boltzmann equation, so that all ions are taken into account explicitly rather than as a mean field.

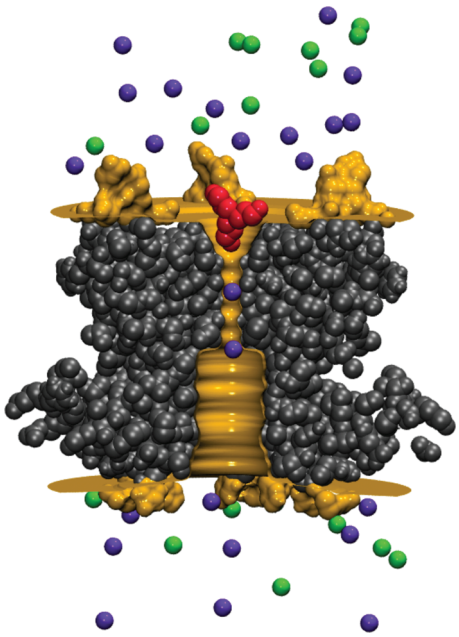

Figure 2. Schematic cutaway representation of the Brownian dynamics simulation. The dielectric boundary is shown in gold and is a hybrid cylindrically symmetric and nonsymmetric surface. Three of the four turret regions can be seen protruding into the extracellular space above the pore. The atoms inside the protein are shown in gray surrounding the pore. Potassium ions are purple and chloride ions are green. The blocker is shown in crimson and can be seen inserted into the mouth of the channel on the extracellular (top) side.

Many of the details of the simulation are well documented in earlier work[29] and will not be reiterated here. We instead concentrate on the new features of our simulation: the inclusion of rigid body blocker molecules and the extension of the pore boundary from a cylindrically symmetric surface to a hybrid surface.

New Electrostatics and Pore Model. Our current work extends previous work[29] by allowing for noncylindrically symmetric regions of the dielectric boundary. In the past, we have employed a cylindrically symmetric pore boundary to represent the nearly cylindrically symmetric channel. However, looking at Figure 2, we see that the Kv1.2 channel protein can be well represented as a bulk cylindrically symmetric region plus some well hydrated "turrets", only a few atoms thick, that protrude into the aqueous medium. Geometrically, these turret regions do not lend themselves well to a cylindrically symmetric representation of the pore boundary. The need for treating the turret regions separately is made the more pressing by the requirement to handle large blocker molecules that may wrap themselves around the turret residues in a way that would be impeded in the symmetrized system.

Unfortunately, though, in order to attain the required computational efficiency to calculate solutions to Poisson's equation for all possible one- and two-ion configurations, we require the use of the boundary element method of solving Poisson's equation combined with a cylindrically symmetric boundary. Being well hydrated, the turrets would not be expected to make much of a contribution to image charge effects due to mobile charges, but certainly the partial charges of their constituent atoms should be taken into account. Hence, we use the symmetric boundary only for calculating the mobile charge image charge effects and the effect of the applied constant electric field, and the combined symmetric/nonsymmetric boundary for calculating the electrostatics that are due to the channel partial charges. The former is achieved with our boundary element method solver and the latter using the Adaptive Poisson–Boltzmann Solver (APBS).[30] We have verified computationally that in the case of a purely cylindrically symmetric pore boundary, the APBS solution is virtually identical to the boundary element method solution, so that there is a certain amount of self-consistency in this approach despite the use of the two solutions. The ions are prevented from crossing the symmetric boundary by the presence of a $1/r^9$ potential whose parameters are set such that the center of the potential lies 1.4 Å behind the boundary, and the force experienced when the surface of an atom touches the boundary is 2×10^{-10} N.

Nonpolar Atom–Atom Interactions. In earlier work,[29,31] we modeled the ion–ion nonpolar interactions using a fitted function which took into account the effect of the hydration shells around the ions. The inclusion of rigid body blocker molecules (as well as a noncylindrically symmetric representation of the pore boundary, see below) in our simulation means that we also need to model the interactions between nonion atoms and other atoms, for which the use of similar fitted potentials is not feasible. As the strong electrostatics are expected to dominate in and around the mouth of the ion channel, and because the blocker considered in this work is small, we do not here consider a detailed treatment of nonpolar solvation forces. It is therefore most appropriate to simply model the hard-core steric forces between atoms to prevent them from overlapping. These interactions are simply modeled using repulsive $1/r^{12}$ potentials, with parameters chosen so as to give thermodynamic equivalence to the case of hard spheres whose radii are equal to the atomic radii[32] as determined by the zero point of the Lennard-Jones potential, namely ε, or

dx.doi.org/10.1021/jp210105f | J. Phys. Chem. B 2012, 116, 1933–1941

$0.89r_{min}/2$. In future versions of our program, we will use a more sophisticated treatment of nonpolar solvation.

The Test Charge Approximation. All forces in the simulation act on the individual atoms, whether these be ions or atoms inside a rigid body molecule. Forces and torques on the rigid bodies therefore arise purely from the combined effect of forces on their constituent atoms. We use a common approximation, known as the "test charge approximation", where the interior of the small blocker molecule is considered to have the same dielectric as the solvent, with its dielectric boundary being ignored. We have found this approximation to be excellent for small molecules like the one used here.

Rigid Body Brownian Dynamics Algorithm. To simulate the rigid blocker molecules, we also need a means to simulate their combined and coupled rotational and translational Brownian motion. For this purpose, we devised an algorithm,[33] for which the geometric algebra of three-dimensional Cartesian space is employed[34] in order to provide an algorithm with better error scaling than the commonly used Euler method.

The position and orientation of a rigid body can be described by a seven-component object $X := (\mathbf{x},R)$, where $\mathbf{x}$ is the center of mass and R is a four-component normalized rotor (or quaternion) describing the rotational orientation of the object around its center of mass. We refer to X as the *generalized position*. Likewise, the *generalized velocity* $V := (\mathbf{v},\Omega)$ is a six-component object, where $\mathbf{v}$ is the center of mass velocity and Ω is the angular velocity, here assumed to be expressed in a reference frame that is relative to the rigid body.

We write down the equations of motion in tensor form. To correctly represent the stochastic calculus, we use the differential form of the equations of motion rather than the usual form expressed in terms of time derivatives. We let $\{X_\alpha\}$ be the seven components of the generalized position, made up of three components of $\mathbf{x}$ and four components of R, and let $\{V_\alpha\}$ be the six components of the generalized velocity, made up of three components of $\mathbf{v}$ and three components of Ω. Also, letting dt be the time differential and dW be the Brownian motion differential, we have the equations of motion

$$dV_\alpha = \{a_\alpha(X) + b_{\alpha\beta n}V_\beta\Omega_n - \gamma_{\alpha\beta}V_\beta\}\,dt + s_{\alpha\beta}\,dW_\beta \quad (1)$$

$$dX_\alpha = \{c_{\alpha nm}R_n\Omega_m + d_{\alpha nmj}R_nR_mv_j\}\,dt \quad (2)$$

We use the convention that the indices α, β, γ range over all translational and rotational coordinates i, j, k range over the translational coordinates only and n, m, l range over rotational coordinates only. The first term on the right-hand side of eq 1 is directly analogous to the usual acceleration term due to all the systematic forces and is in general nonlinear in X. The second term is a geometric term arising from the algebra of rotations and does not have an analogy in the motion of point particles. It could be likened to the Coriolis force. The third term is a frictional acceleration term. Unlike the case of a point particle, the friction coefficient γ is now a tensor rather than a scalar, whose elements depend on the details of the rigid body and must be determined e.g. by hydrodynamic calculations. The fourth term is the random force term, with the tensor s being related to γ by a fluctuation−dissipation result. Moving to the equation for X, eq 2, the first term $c_{\alpha nm}R_n\Omega_m\,dt$ comes from the *rotor equation* and represents the rotation of a body under an angular velocity. The second term $d_{\alpha nmj}R_nR_mv_j\,dt$ is simply derived from $d\mathbf{x} = \mathbf{v}\,dt$, with the addition of rotations from the frame of reference of the body to the laboratory frame.

We model our algorithm on the velocity Verlet algorithm, but the addition of terms dependent on V in eq 2 means that the usual algorithm cannot be directly applied, and the more complicated rotational structure of the equations means that an analytically based extension, such as that of van Gunsteren and Berendsen,[35] also cannot be found. Instead, we apply the following algorithm:

1. Calculate $X(t_{n+1})$ based on the values of $X(t_n)$ and $V(t_n)$.
2. Evaluate the potential at the new X, $a(X(t_{n+1}))$.
3. Use the newly evaluated position and potential to derive the new velocity, $V(t_{n+1})$. Because of the presence of V on the rhs of eq 1, the equation we derive is of the form $V(t_{n+1}) = f(a(X(t_{n+1})),X(t_{n+1}),V(t_{n+1})$ and must be solved iteratively due to the presence of $V(t_{n+1})$ on the rhs.

The error of this algorithm scales as $\Delta t^{5/2}$, compared to $\Delta t^{3/2}$ for the simpler Euler algorithm.

The algorithm depends on both the moment of inertia tensor and the frictional tensor of the rigid body being simulated. The former is simply calculated using the coordinates and masses of the constituent atoms, while the second is in general hard to calculate; we use the HYDROPRO program of de la Torre et al.[36] which applies hydrodynamics to the problem.

Potentials of Mean Force from Brownian and Molecular Dynamics. To derive the potential of mean force (PMF) of the blocker/channel interaction in Brownian dynamics, a series of umbrella sampling runs are performed using umbrella windows placed at 1 Å intervals. For each window, the z-component of the center of mass of the blocker is constrained to the window location using a harmonic potential with spring constant of 5 kcal/(mol Å^2). To ensure convergence of the PMF, each window is run for a total of around 17 ns. The z-component of the center-of-mass trajectory of the blocker is collected at 10 ps intervals. To derive a meaningful one-dimensional potential of mean force, the blocker is also constrained by a flat-bottomed harmonic potential, which is zero inside an 8 Å radius and sharply rising outside that radius, in order to constrain the center of mass of the blocker to lie within 8 Å of the pore axis. Care must be taken when interpreting one-dimensional PMFs, which are only really physically meaningful in regions where the blocker is radially constrained by the channel. The trajectory data are then analyzed using the weighted histogram analysis method (WHAM).[37]

A similar procedure is followed for the molecular dynamics simulation, except that the umbrella sampling windows are placed at 0.5 Å intervals in the region near to the channel and at 1 Å intervals at distances larger than 26 Å from the channel center of mass. Umbrella constraints are applied using a spring constant of 20 kcal/(mol Å^2) for the windows spaced at 0.5 Å intervals and 10 kcal/(mol Å^2) for the windows spaced at 1 Å intervals, by means of the "colvars" feature of NAMD. The reaction coordinate is the projection of the center-of-mass displacement vector between the blocker and channel onto the z-axis (which closely corresponds to the channel axis); the NAMD "colvars" module then obtains the forces by calculating derivatives of the reaction coordinate with respect to the Cartesian coordinates of each atom. Similar to the Brownian dynamics case, an additional flat-bottomed potential holds the blocker within an 8 Å radius of the z-axis. Each widow is run for 5 ns. Similar techniques were employed by Chen and Kuyucak[16,17] to determine the PMFs of polypeptide toxins unbinding from potassium channels.

RESULTS AND DISCUSSION

Channel Equilibration and Stability. The channel is found to be relatively stable during the second half of the 10 ns of equilibration, with a backbone rmsd of 0.9 Å and an overall rmsd of 1.2 Å. The turret loop, residues 350−358, is somewhat more mobile, due to the fact that it is an unstructured loop and can drift around relatively freely in the extracellular medium. It is found to have a backbone rmsd of 1.1 Å and an overall rmsd of 1.6 Å. The carbonyl oxygens that line the selectivity filter remain in their pore-facing configuration, and the ions and water that were initially placed in the channel remain in their initial configuration, with the ions occupying binding sites S0 (just above Tyr377), S2 (between Gly376 and Val375), and S4 (just below Thr374), which is consistent with previous work.[38−40] The equilibrated channel is shown in Figure 3. Note the differently oriented side chains of the Asp379 residues.

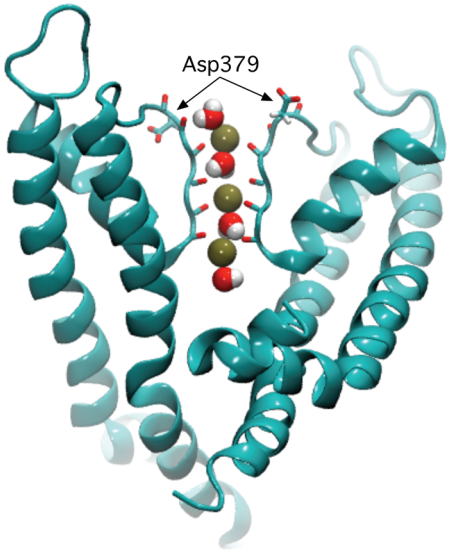

Figure 3. The equilibrated channel, taken from molecular dynamics calculations, showing the selectivity filter with K^+ ions at binding sites (from top to bottom) S0, S2, and S4, separated by water molecules. For clarity, only two segments of the channel tetramer are shown. The carbonyl oxygen atoms of the selectivity filter are shown in licorice representation, as are the side chains of the Asp379 residues, seen near the top of the selectivity filter.

Spontaneous Binding of the Blocker during Molecular Dynamics Simulations. The blocker is placed about 15 Å from the pore entrance and is allowed to freely move toward the channel. During the 5 ns simulation, the blocker moves toward the pore and is initially seen to interact with the Asp379 residues that surround the pore before inserting one leg into the pore while also maintaining a close interaction with the aspartate residues. The bound configuration is shown in Figure 4, with the binding sequence being shown as Figure S1 in the Supporting Information. This sequence of events was seen to occur in two independent simulations. The hydrogen bond is formed either to the carbonyl oxygen or to the OD1 or OD2 oxygens. Typically the aspartate side chain is more or less flipped up so that it faces the extracellular medium.

Brownian Dynamics Channel Model. Given that the channel model in Brownian dynamics is fixed, rigid entity that approximates the moving protein, it is necessary to choose a particular protein configuration to construct the channel. We therefore investigate the effects of three types of changes to the protein, in order to optimize (a) the conductance of the channel, (b) the fact that the channel exhibits simultaneous binding of ions at binding sites S0, S2, and S4 and (c) the binding of the blocker, as seen in molecular dynamics simulations. Our optimized channel has a very slightly expanded selectivity filter, an expanded inner vestibule, and has the Asp379 residue rotated out to face away from the bulk of the channel.

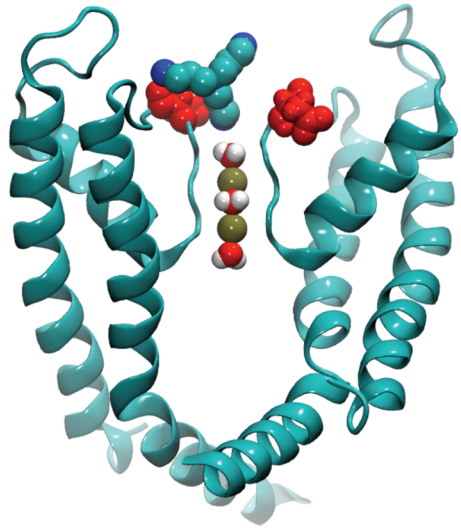

Figure 4. The channel/blocker system in a typical bound configuration, taken from molecular dynamics calculations. Two of the four Asp379 residues are depicted in red, and the blocker can be seen between them; the K^+ ions and water inside the filter are also shown. The blocker inserts one leg into the pore, with its nitrogen center approximately at position S0. It tilts off center in order to form close contacts with the Asp379 residue.

The first modification, the expansion of the selectivity filter, is used in order to accommodate the movement of ions through the rigid Brownian dynamics channel; we ensure that the filter is of sufficient size to fit K^+ ions; around 1.3−1.4 Å. Second, channel conductance is known to depend strongly on the width of the vestibule,[29,41,42] which can vary[40] and probably forms a key part of the gating mechanism. Furthermore, the vestibule is somewhat square in cross section, and our symmetrized model for the pore may therefore underestimate its volume. We therefore treat the width of the inner vestibule as an adjustable parameter and expand it somewhat in order to optimize the channel conductance. Figure 5A shows the pore shape with and without the expansions of the inner vestibule and selectivity filter detailed above. The chosen expansions give rise to a model that shows a conductance that is compatible with experiment. The inner vestibule expands in radius by between 1 and 2 Å, while the filter expands by only a fraction of an angstrom.

Third, our molecular dynamics simulations show that the side chains of the Asp379 residues often face away from the pore and into the extracellular medium during their interaction with the blocker molecule. In the initial crystal structure, the side chain faces in toward the protein, so that the charges are somewhat buried. We find that, in our Brownian dynamics model, the orientation of these charged side chains plays an important role in the electrostatics at the mouth of the channel that can affect the strength of the binding of the blocker and the

dx.doi.org/10.1021/jp210105f | J. Phys. Chem. B 2012, 116, 1933−1941

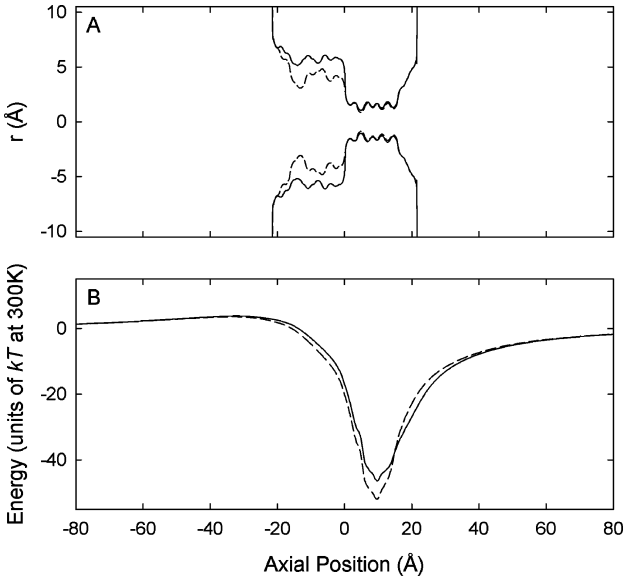

Figure 5. (A) Pore model used for the symmetric pore boundary in Brownian dynamics. The solid curve shows the actual pore model after refinement and molding, and the broken curve shows the pore prior to these changes. (B) Single-ion energy profiles, with the solid curve having the Asp379 residue facing away from the bulk of the protein and the broken curve having it facing inward. The horizontal scale gives the location of the ion along the axis of the channel.

presence of a significant ion binding site at the S0 position. Figure 5B compares the single ion energy profiles of the system with two orientations of the Asp379 residue. The curve corresponding to the flipped out aspartate residues shows a deeper well near the entrance to the selectivity filter but a shallower well overall. The flipped-out orientation of the aspartate side chain, as is seen during the binding of the blocker in molecular dynamics, is needed in order to see a similar binding mode in Brownian dynamics, with one arm of the blocker interacting with Asp379 while the other inserts into the pore.

Comparison of Molecular Dynamics and Brownian Dynamics Potentials of Mean Force. The potentials of mean force, derived using both Brownian and molecular dynamics as outlined in the Methods section, are shown in Figure 6. The convergence of the PMFs as well as snapshots of the blocker at various molecular dynamics umbrella windows are also shown as Figures S2 and S3 in the Supporting Information. It is clear that the well depths as well as the medium- and long-range electrostatics agree remarkably well, but that the details of the binding itself differ somewhat, with the molecular dynamics PMF showing a pronounced plateau region between z = 23 and 26 Å and a very tight binding pocket at z = 22 Å, while the PMF for the Brownian dynamics simulation drops more uniformly to a somewhat broader binding pocket.

By examining the details of the molecular dynamics trajectories, it is clear that the plateau in the PMF corresponds to a binding mode that has two legs of the blocker bound to adjacent Asp379 residues while the other leg is free to pivot up and down in the solution. The pivoting accounts for the fact that the PMF plateaus, since the center of mass of the blocker can move in and out via this pivoting motion while the two legs remain in close contact with the aspartate residues, accounting for the bulk of the electrostatic and nonpolar interaction

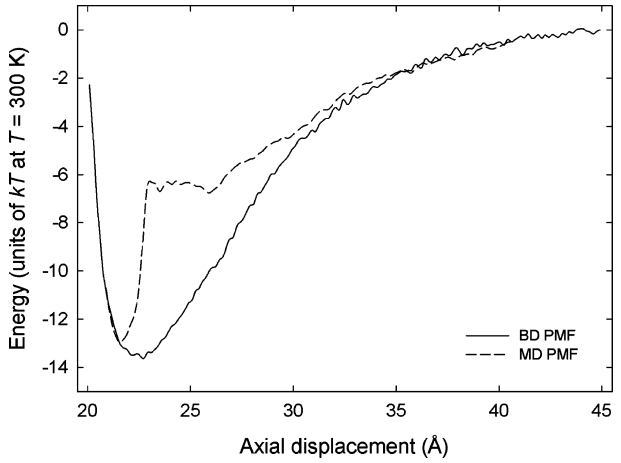

Figure 6. Potentials of mean force for the blocker binding to the channel, as derived using molecular and Brownian dynamics.

energy. Clearly, the fine details of the interaction and the balance between competing energies mean that in the Brownian dynamics simulation this binding mode is not as prominent. In terms of binding and blocking, this difference in the PMFs might mean that the blocker would be more tightly bound to the channel in molecular dynamics, and hence the blocked channel might be expected to be less leaky to ions but that overall binding affinity would be slightly greater in Brownian dynamics.

We calculate the dissociation constant K_d from the PMF according to the usual relation as

$$K_d^{-1} = 1000\pi R^2 N_A \int_{z_1}^{z_2} \exp(-W(z)/kT)\, dz \quad (3)$$

where z_1 and z_2 give the limits of the binding site, $W(z)$ is the one-dimensional PMF, with the zero point of energy set to be zero in the bulk, N_A is Avogadro's number, k is Boltzmann's constant, and T is the temperature. The factor of $1000N_A$ is a conversion from m^3 to L/mol. Applying this calculation to the PMFs above, we find a dissociation constant of 4.7 μM for the Brownian dynamics calculation and 22 μM for the molecular dynamics calculation, with the two results differing by a factor of 4.7, or 1.5 kT when expressed in terms of free energy of binding. In terms of binding affinity, this places the blocker somewhere in between the polypeptide toxins, with binding constants in the nanomolar to picomolar range, and tetraethylammonium externally blocking the Shaker channel, with a binding constant of around 1 mM,[43] which is not surprising as the blocker appears to share features of both the toxins and tetraethylammonium.

Block of the Channel in BD. We use Brownian dynamics to investigate the effect of the blocker on channel permeation. Sixteen anions and 16 cations are placed in the top reservoir and the same number in the bottom reservoir, giving a concentration of ~320 mM KCl. Constant electric fields are applied to the system using various solutions to Poisson's equation, corresponding to varying membrane potentials. In one set of runs, a single blocker molecule is placed in the upper reservoir (giving a concentration of 20 mM). For each run, approximately 1−2 μs of data is collected.

The current−voltage curves are shown in Figure 7. The control curve is nearly straight between ±200 mV and exhibits a chord conductance of 15 pS between 0 and 100 mV. This is

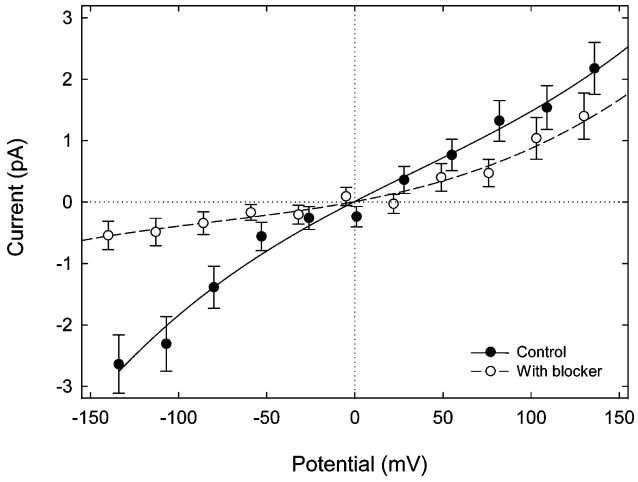

Figure 7. Current−voltage curves for the control system (solid line) and the system with a single blocker (broken line).

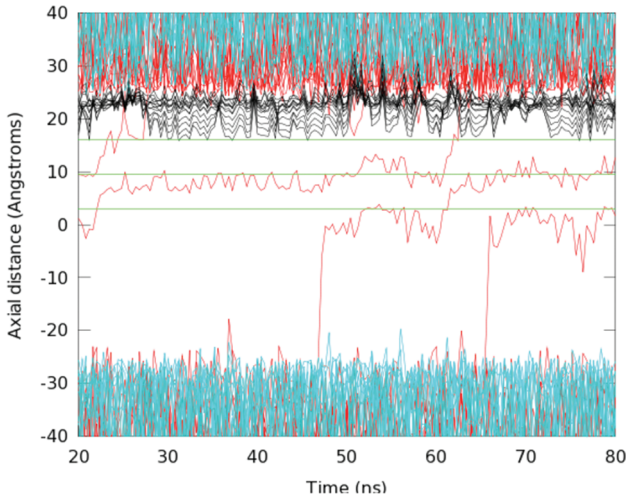

Figure 8. A Brownian dynamics trajectory, showing outward conduction occurring despite the presence of the blocker. Time is on the horizontal axis and the axis of the channel, z is the vertical axis. Anions are shown in blue, cations in red, and the atoms in the blocker in black. The binding sites S0, S2, and S4 are shown as green horizontal lines, moving from the top to the bottom of the figure in the order given. The channel runs from around $z = -25$ Å to $z = 25$ Å. At any given time, there are either one or two red K^+ in the pore, plus the black blocker bound to the mouth of the pore, most of the time with one of its legs inserted into the pore down to around $z = 17$. The positively charged amide group of blocker in the pore acts as a proxy for a third ion in the S0 binding site. Between 45 and 65 ns, a K^+ ion can be seen moving into the inner vestibule of the pore and from thence into the bottom of the selectivity filter, displacing another ion upward and causing a conduction to occur via a knock-on process. During conductions, the blocker lifts out of the pore entrance slightly, thus making room for the upward passage of the ion in binding site S2. Following the conduction, another ion traverses the inner vestibule and moves into the bottom of the filter, thus priming the channel for another conduction to take place.

similar to experimentally measured conductances which range from 18 pS for Kv1.2[44−46] to 33 pS at 300 mM for shaker (Kv1.0).[47] The presence of the blocker reduces the current at all voltages, while also causing the curve to become markedly outward rectifying. The block at +100 mV is about 33%, while it is about 74% at −100 mV.

The fact that the inward current is more effectively blocked than the outward current can easily be explained by noting that at negative membrane potentials, the blocker will be more tightly bound to the channel. Also, an ion moving upward from the selectivity filter will tend to force the blocker away from the entrance to the filter, thus decreasing the effectiveness of the block, while an inwardly conducting ion will either have little effect on the blocker or will have the opposite effect.

Earlier, we gave a value of 4.7 μM for the dissociation constant, meaning that at the simulation blocker concentration of 20 mM the blocker should nearly always be bound to the channel. Indeed, this is the case in our simulations. Therefore, the only partial block must result from a "leaky blocker", where ions leak through the channel despite the presence of the bound blocker. This can be seen in Figure 8, which under careful examination shows the conductions occurring in the intervals when the blocker slightly pulls away from the pore. The leakiness of the block can be related to the shape of the external vestibule of the Kv1.2 channel, which is broad and open and lacks the "binding cage" seen in KcsA, into which tetraethylammonium can lodge, blocking that channel.[48−50] Any minor lifting of the blocker out of the entrance to the selectivity filter provides an opportunity for the passage of ions. It is interesting to speculate that the large polypeptide toxins avoid this leakiness first by their large bulk and second by tightly binding to the entrance to the channel with at least two salt bridges formed to the negatively charged residues surrounding the pore combined with the insertion of a lysine into the pore entrance. We also speculate that extending the blocker molecule so that it can form an additional salt bridge to one of the Asp379 residues would improve the effectiveness of the block. Lastly, looking back to the PMFs shown in Figure 6, we see that the molecular dynamics PMF appears to show a narrower binding pocket, and hence our Brownian dynamics simulations might overestimate the leakage of ions from the blocked channel.

Molecular dynamics simulations show that the blocker molecule is relatively rigid, as expected due to its small size. Furthermore, it binds to a rigid region of the protein that is devoid of long isolated side chains. Hence, considerations of protein flexibility are not expected to play the crucial role in the binding characteristics. The situation is somewhat different for larger molecules, including polypeptide venom channel blockers. Such molecules contain multiple flexible side chains that can interact with other flexible portions of the protein such as the turret regions. In such cases, a fully rigid treatment like the one given in this paper may suffer from the same problems faced by rigid body protein−protein docking programs,[51] and the induced fit of a flexible treatment may significantly alter the free energy of binding. The use of partially flexible rigid-body Brownian dynamics, either employing molecular dynamics type bond parameters or even more sophisticated treatments of coupled rigid bodies,[52] could be an interesting new area of exploration.

■ CONCLUSIONS

We have demonstrated a means to simulate the interaction of ions and other rigid-body molecules interacting with an ion channel using Brownian dynamics. Testing this system on the Kv1.2 channel and using a polyamine analogue of spermine as a blocker molecule, we have found that the blocker binds to the channel in both Brownian and molecular dynamics simulations.

dx.doi.org/10.1021/jp210105f | J. Phys. Chem. B 2012, 116, 1933−1941

The binding mechanism appears to mimic features of the way polypeptide toxins such as charybdotoxin interact with the channel, with an overall electrostatic attraction combined with the insertion of an amine group into the pore entrance and the interaction of another with one of the aspartate residues that surround the pore. We find that the Brownian dynamics and molecular dynamics potentials of mean force are in reasonable agreement, with nearly the same well depth and unbound curves, but showing a difference in the shape of the curves in the region where the blocker directly interacts with the pore entrance. Using Brownian dynamics to construct current−voltage profiles for the system with and without the blocker, we find that despite the fact that it binds strongly to the channel, the blocker is only partially effective at blocking the passage of K^+ ions through the channel, causing around 1/3 block at positive voltages and 3/4 block at negative voltages.

It should be possible to extend this molecule to provide an additional contact with another channel aspartate, leading the blocker to bind more tightly to the mouth of the pore and increasing the effectiveness of the blockade. In future work, we intend to refine the model of the blocker/channel interactions to more faithfully model the process of block by implementing a more sophisticated treatment of nonpolar interactions. We also intend to investigate the introduction of a degree of flexibility into the molecular models. Using this system, we will look for extensions to the blocker that will give rise to a more effective block as well as investigating other channels and other blocker molecules, both small synthetic molecules and polypeptides. Establishing the general applicability of our methods to small and even large blocker molecules would provide an extremely useful new tool, which could have important applications in drug development as well as basic ion channel research.

■ ASSOCIATED CONTENT

Supporting Information

Figure S1: the spontaneous binding of the blocker to the channel in molecular dynamics simulations; Figure S2: the convergence of the PMFs; and Figure S3: positions of the blocker in various molecular dynamics umbrella sampling windows. This material is available free of charge via the Internet at http://pubs.acs.org.

■ AUTHOR INFORMATION

Corresponding Author

*E-mail: dan.gordon@anu.edu.au.

■ ACKNOWLEDGMENTS

The calculations upon which this work is based were carried out using a SGI Altix 3700 system of the Australian National University Supercomputer Facility. This work is supported by grants from the NHMRC and the MAWA Trust. M.L.C. gratefully acknowledges an ARC Future Fellowship.

■ REFERENCES

(1) Shieh, C. C.; Coghlan, M.; Sullivan, J. P.; Gopalakrishnan, M. *Pharmacol. Rev.* **2000**, *52*, 557−594.
(2) Ren, Y. R.; Pan, F.; Parvez, S.; Fleig, A.; Chong, C. R.; Xu, J.; Dang, Y.; Zhang, J.; Jiang, H.; Penner, R.; Liu, J. O. *PLoS One* **2008**, *3*, e40091−11.
(3) Beeton, C.; Pennington, M. W.; Wulff, H.; Singh, S.; Nugent, D.; Crossley, G.; Khaytin, I.; Calabresi, P. A.; Chen, C.-Y.; Gutman, G. A.; Chandy, K. G. *Mol. Pharmacol.* **2005**, *67*, 1369−1381.
(4) Kalman, K.; Pennington, M. W.; Lanigan, M. D.; Nguyen, A.; Rauer, H.; Mahnir, V.; Paschetto, K.; Kem, W. R.; Grissmer, S.; Gutman, G. A.; Christian, E. P.; Cahalan, M. D.; Norton, R. S.; Chandy, K. G. *J. Biol. Chem.* **1998**, *273*, 32697−32707.
(5) Rauer, H.; Pennington, M.; Cahalan, M.; Chandy, K. G. *J. Biol. Chem.* **1999**, *274*, 21885−21892.
(6) Beeton, C.; Smith, B. J.; Sabo, J. K.; Crossley, G.; Nugent, D.; Khaytin, I.; Chi, V.; Chandy, K. G.; Pennington, M. W.; Norton, R. S. *J. Biol. Chem.* **2008**, *283*, 988−997.
(7) Abagyan, R.; Totrov, M. *Curr. Opin. Chem. Biol.* **2001**, *5*, 375−382.
(8) Halperin, I.; Ma, B.; Wolfson, H.; Nussinov, R. *Proteins* **2002**, *47*, 409−443.
(9) Long, S. B.; Campbell, E. B.; Mackinnon, R. *Science* **2005**, *309*, 897−903.
(10) Park, C. S.; Miller, C. *Biochem.* **1992**, *31*, 7749−7755.
(11) Park, C. S.; Miller, C. *Neuron* **1992**, *9*, 307−313.
(12) Goldstein, S. A.; Miller, C. *Biophys. J.* **1993**, *65*, 1613−1619.
(13) Aiyar, J.; Withka, J. M.; Rizzi, J. P.; Singleton, D. H.; Andrews, G. C.; Lin, W.; Boyd, J.; Hanson, D. C.; Simon, M.; Dethlefs, B. *Neuron* **1995**, *15*, 1169−1181.
(14) Doyle, D. A.; Cabral, J. M.; Pfuetzner, R. A.; Kuo, A.; Gulbis, J. M.; Cohen, S. L.; Chait, B. T.; MacKinnon, R. *Science* **1998**, *280*, 69−77.
(15) Yu, K.; Fu, W.; Liu, H.; Luo, X.; Chen, K. X.; Ding, J.; Shen, J.; Jiang, H. *Biophys. J.* **2004**, *86*, 3542−3555.
(16) Chen, P. C.; Kuyucak, S. *Biophys. J.* **2009**, *96*, 2577−2588.
(17) Chen, P. C.; Kuyucak, S. *Biophys. J.* **2011**, *100*, 2466−2474.
(18) Humphrey, W.; Dalke, A.; Schulten, K. *J. Mol. Graphics* **1996**, *14*, 33−38.
(19) Phillips, J. C.; Braun, R.; Wang, W.; Gumbart, J.; Tajkhorshid, E.; Villa, E.; Chipot, C.; Skeel, R. D.; Kalé, L.; Schulten, K. *J. Comput. Chem.* **2005**, *26*, 1781−1802.
(20) Han, M.; Zhang, J. Z. H. *J. Phys. Chem. B* **2008**, *112*, 16966−16974.
(21) MacKerell, A. Jr.; et al. *J. Phys. Chem. B* **1998**, *102*, 3586−3616.
(22) Mackerell, A. D. Jr.; Feig, M.; Brooks, C. L. III *J. Comput. Chem.* **2004**, *25*, 1400−15.
(23) Frisch, M. J.; Trucks, G. W.; Schlegel, H. B.; Scuseria, G. E.; Robb, M. A.; Cheeseman, J. R.; Montomery, Jr., J. A.; Vreven, T.; Kudin, K. N.; Burant, J. C.; et al. *Gaussian 03, Revision C.02*; Gaussian, Inc.: Wallingford, CT, 2004.
(24) Reed, A. E.; Weinstock, R. B.; Weinhold, F. *J. Chem. Phys.* **1985**, *83*, 735−746.
(25) Reed, A. E.; Weinhold, F. *J. Chem. Phys.* **1985**, *83*, 1736−1740.
(26) Foster, J. P.; Weinhold, F. *J. Am. Chem. Soc.* **1980**, *102*, 7211−7218.
(27) Klamt, A.; Schürmann. *J. Chem. Soc., Perkin Trans. 2* **1993**, *5*, 799−805.
(28) Cossi, M.; Rega, N.; Scalmani, V. B. *J. Comput. Chem.* **2003**, *24*, 669−796.
(29) Chung, S.-H.; Allen, T. W.; Kuyucak, S. *Biophys. J.* **2002**, *82*, 628−645.
(30) Baker, N. A.; Sept, D.; Joseph, S.; Holst, M. J.; McCammon, J. A. *Proc. Natl. Acad. Sci. U. S. A.* **2001**, *98*, 10037−10041.
(31) Corry, B.; Allen, T. W.; Kuyucak, S.; Chung, S.-H. *Biophys. J.* **2001**, *80*, 195−214.
(32) Hansen, J. P.; McDonald, I. R. *Theory of Simple Liquids*, 3rd ed.; Academic Press: London, 2006; p 118.
(33) Gordon, D.; Hoyles, M.; Chung, S.-H. *Phys. Rev. E* **2009**, *80*, 066703 1−12.
(34) Doran, C.; Lasenby, A. *Geometric Algebra for Physicists*; Cambridge University Press: Cambridge, 2003.
(35) van Gunsteren, W.; Berendsen, H. J. C. *Mol. Phys.* **1982**, *45*, 637−647.
(36) de la Torre, J. G.; Huertas, M. L.; Carrasco, B. *Biophys. J.* **2000**, *78*, 719−730.

(37) Grossfield, A. Weighted Histogram Analysis Method. http://membrane.urmc.rochester.edu/content/wham (accessed Dec 11, 2011).
(38) Yu, L.; Sun, C.; Song, D.; Shen, J.; Xu, A., N.; Gunasekera; Hajduk, P. J.; Olejniczak, E. T. *Biochemistry* **2005**, *44*, 15834−15841.
(39) Khalili-Araghi, F.; Tajkhorshid, E.; Schulten, K. *Biophys. J.* **2006**, *91*, L72−L74.
(40) Jensen, M. Ö.; Borhani, D. W.; Lindorff-Larsen, K.; Maragakis, P.; Jogini, V.; Eastwood, M. P.; Dror, R. O.; Shaw, D. E. *Proc. Natl. Acad. Sci. U. S. A.* **2010**, *107*, 5833−5838.
(41) Korn, S. J.; Trapani, J. G. *IEEE Trans. Nanobiosci.* **2005**, *4*, 21−33.
(42) Li, W.; Aldrich, R. W. *J. Gen. Physiol.* **2004**, *124*, 43−57.
(43) Heginbotham, L.; MacKinnon, R. *Neuron* **1992**, *8*, 483−491.
(44) Conforti, L.; Millhorn, D. E. *J. Physiol.* **1997**, *502* (Pt.2), 293−305.
(45) Conforti, L.; Bodi, I.; Nisbet, J. W.; Millhorn, D. E. *J. Physiol* **2000**, *524* (Pt 3), 783−793.
(46) Grissmer, S.; Nguyen, A. N.; Aiyar, J.; Hanson, D. C.; Mather, R. J.; Gutman, G. A.; Karmilowicz, M. J.; Auperin, D. D.; Chandy, K. G. *Mol. Pharmacol.* **1994**, *45*, 1227−1234.
(47) Heginbotham, L.; MacKinnon, R. *Biophys. J.* **1993**, *65*, 2089−2096.
(48) Crouzy, S.; Bernéche, S.; Roux, B. *J. Gen. Physiol.* **2001**, *118*, 207−217.
(49) Bisset, D.; Chung, S.-H. *Biochim. Biophys. Acta* **2008**, *1778*, 2273−2282.
(50) Hoyles, M.; Krishnamurthy, V.; Siksik, M.; Chung, S.-H. *Biophys. J.* **2008**, *94*, 366−378.
(51) Brooijmans, N.; Kuntz, I. *Annu. Rev. Biophys. Biomol. Struct.* **2003**, *32*, 335−373.
(52) Hestenes, D.; Fasse, E. D. In *Applications of Geometric Algebra in Computer Science and Engineering*; Dorst, L., Doran, C., Lasenby, J., Eds.; Birkhäusser: Boston, 2002; pp 197−212.